

## The Effects of Alloying Elements on the Microstructure of Al-Zn alloy

Thi Ngoc Mai Bui<sup>a</sup>, Minh Thai Duong<sup>b</sup>, Van Phuc Nguyen<sup>c</sup>, Duc Chuan Nguyen<sup>c</sup>, Thanh Nam Dang<sup>d,\*</sup>

<sup>a</sup> School of Mechanical Engineering, Vietnam Maritime University, Haiphong, Vietnam

<sup>b</sup> Institute of Mechanical Engineering, Ho Chi Minh City University of Transport, Ho Chi Minh, Vietnam

<sup>c</sup> Institute of Maritime, Ho Chi Minh City University of Transport, Ho Chi Minh, Vietnam

<sup>d</sup> Center of Human Resources & Maritime Training, Ho Chi Minh City University of Transport, Ho Chi Minh, Vietnam

Corresponding author: \*nam.dang@ut.edu.vn

**Abstract**—The effects of alloying elements and rare earth elements such as Zr, Sc, Er, etc., are presented. Structural analysis shows that these rare earth elements all form an intermetallic phase with Al, with the same formula Al<sub>3</sub>RE. This intermetallic phase plays a role in preventing the formation of harmful phases in the alloy. These intermetallic phases can be located within the grain, acting as heterogeneous nucleation centers or at the grain boundary, blocking positions to prevent grain growth. The research presented the roles of the intermetallic phase as the crystallization seed center and the intermetallic phase as the inhibitory phase for grain growth. XRD analysis results have determined the structure of these intermetallic phases, showing their conformity with the background phase. Through theoretical and experimental studies, the deformation and uniform annealing process for the Al-Zn-Mg-Cu alloy was determined in the presence of La and Ce grain refiners. The uniform annealing process removed the dendritic structures after casting and determined the intermetallic phases' role in preventing the matrix phase's growth. XRD analysis results confirmed the structure of the intermetallic phases, demonstrating their conformity with the matrix phase. Research about the influence of rare earth elements in the grain reduction process will help establish a grain reduction protocol for studying alloys during both the melting and homogenization annealing stages. This is particularly crucial for creating high mechanical strength and superplastic alloys within this alloy group.

**Keywords**—Intermetallic phase; rare earth elements; crystallization seed; stable phase; heterogeneous nucleation; Al-Zn alloy.

Manuscript received 12 Mar. 2024; revised 29 Jun. 2024; accepted 17 Jul. 2024. Date of publication 31 Aug. 2024.  
IJASEIT is licensed under a Creative Commons Attribution-Share Alike 4.0 International License.



### I. INTRODUCTION

Industry development has led to the development of technology and materials engineering. Among the materials, metal materials such as steel, aluminum alloys, and copper alloys are commonly used in the fields of industrial production, construction, and transportation [1]–[7]. For steel, there are many studies conducted to improve its mechanical properties, such as alloying solutions, heat treatment, or using modifiers [8]–[17]. However, the solutions for non-ferrous alloys have not been analyzed comprehensively. Being non-ferrous alloys, the Al-Zn alloy is a base alloy with aluminum (Al) as the primary element and zinc (Zn) as the main alloying element, while other alloying elements include magnesium (Mg) and copper (Cu) [18]–[20]. With characteristics such as high castability, good strength, and lower melting temperature, the Al-Zn alloy was developed to compete with copper, cast iron, and aluminum [21]–[25]. This aluminum alloy has significant potential and is utilized in aerospace,

weapon manufacturing, and sports equipment production. Studying fine-grain Al-Zn alloys using rare earths, combined with technological methods suited to local conditions and equipment, requires thorough research to produce high-ductility alloys. The goal is to develop new materials for manufacturing thin parts in industries such as automotive, motorcycle, computer, and phone manufacturing [26]–[30]. This will help increase the localization rate and promote the application of high-ductility alloys in these industries [31]–[33].

Aluminum alloys exhibit vastly different crystallization properties depending on their composition. As a result, the use of grain refining agents varies for each alloy. Without grain refining agents, pure aluminum requires a supercooling of 3–4°C for nucleation to occur. However, once the first crystals reach an acceptable size, the thermite reaction causes the liquid metal temperature to rise again, preventing the formation of new crystallization nuclei [34], [35]. This leads to large, coarse columnar grain growth during solidification. Modifying aluminum alloys serves two main purposes:

refining the primary aluminum grains and refining the secondary grains. Under normal solidification conditions, most aluminum alloys develop a three-zone structure: a delicate outer shell, a layer of columnar dendritic crystals, and coarse, regular dendritic crystals at the center of the casting. The grain coarseness and the length of cylindrical crystals depend on the pouring temperature, the temperature gradient in the mold, and the number of nucleation centers formed during crystallization.

Adding alloying elements to liquid aluminum typically reduces the grain size [36], [37]. Alloys containing elements with good solubility, such as Cu, Mg, and Zn, are easier to modify regarding grain size than those containing only silicon. For example, modifying Al-Si-Mg-Cu alloys can result in small and refined grains. However, in Al-Si alloys with high silicon content, grain refinement is more challenging due to silicon's high growth inhibition coefficient [36], [38]–[41]. Thermodynamically, the crystallization process of metals involves two stages: nucleation and nucleation growth. The nucleation and growth rates of the nuclei are critical parameters that determine the structure and properties of the alloy. The main goal of modification is to influence these two parameters [36], [37], [42].

A solid solution  $\beta$  based on zinc dissolves aluminum in small quantities. At 382°C, the solubility of aluminum in  $\beta$  is approximately 1.1%. At this temperature, with an aluminum content of 5%, a reaction occurs alongside the solid solution [31], [43]:



In the  $\alpha$  phase, there is 79% zinc. Rapid cooling can maintain this supersaturated concentration in  $\alpha$  at room temperature. Upon slow cooling, a favorable reaction will occur [31], [43]:



The Al-Zn alloy has excellent castability and high mechanical properties in the cast state. At low temperatures, the  $\alpha$  phase will precipitate the  $\beta$  phase with the same composition as pure Zn because Al dissolves in Zn very minimally, only about 2%. However, at 380°C, Zn can dissolve up to 84%. The  $\alpha$  and  $\beta$  phases form a coarse microstructure during normal solidification without intervention. To overcome the coarse structure of the  $\alpha$  and  $\beta$  phases, measures must be taken to refine the granularity and improve the alloy's microstructure, according to the Hall-Petch equation [44]–[49]:

$$\sigma = \sigma_0 + k \cdot \frac{1}{\sqrt{d}} \quad (3)$$

In this context:

- $\sigma_0$  represents the stress needed to initiate deviation.
- $d$  stands for particle size.
- $k$  denotes lattice constant.

The alloy's strength improves with smaller grain sizes. To achieve finer grain structure, refining methods are employed during casting to achieve the desired structure. This article explores the impact of critical elements and rare earth elements on the microstructure of Al-Zn alloy.

### A. Materials

The alloy studying belongs to the Al-Zn-Mg-Cu system, closely resembling the 7475 (AA) alloy grade, classified among high-strength deformed aluminum alloys. Table 1 details the composition of this alloy.

TABLE I  
CHEMICAL COMPOSITION OF THE STUDIED ALLOY [50]

Elements	Zn	Mg	Cu	Si	Fe	Mn	La	Ce	Al
Sample 1	8.26	2.3	1.11	0.7	0.15	0.12	x	x	remaining
Sample 2	7.6	1.9	1	0.6	0.19	0.17	0.21	0.155	remaining

1) *Ingredients for preparing aluminum ingots:* To prepare aluminum ingots for the experiment, follow these steps: First, ensure each ingot weighs approximately 7-8 kg. Next, cut the aluminum billets into small pieces to fit into the cooking pot, aiming for batches weighing around 1-1.2 kg each. After cutting, thoroughly clean the workpieces to remove dust, then dry them at 200°C to eliminate any remaining surface moisture. Additionally, pure metals should be included to achieve the desired composition for each batch. Pure zinc (Zn) and magnesium (Mg) should be chopped and dried with aluminum ingots before smelting. [50].

2) *Grain refiner preparation:* The grain refiner utilized consists of rare earth elements, primarily La (lanthanum) and Ce (cerium). The rare earth pieces are first sawed into small segments to form intermediate alloy components. Due to the tendency of rare earths to ignite during fine sawing, continuous cooling with water is necessary. After sawing, the rare earth segments are dried on the furnace surface to ensure they are moisture-free before use. [50]–[53]. Commercial cryolite slag salt, constituting 3% of the mass of the processed aluminum in each batch, is utilized. Before addition to the batch, this salt undergoes drying at 200°C to ensure it is free from moisture [54], [55].

3) *Laboratory instruments:* Medium-frequency furnace: This type of induction electric furnace is versatile, used for quenching and tempering mechanical parts, melting metals, and heating billets for forging and pressing. Medium-frequency furnaces operate by inducing currents that generate heat to melt metals efficiently.

4) *Cooking pot:* The cooking pot used in the process is a graphite pot housed within an iron frame, designed for easy handling and manipulation. The graphite pot serves to reduce the iron content that may enter the liquid aluminum, minimizing harmful effects as previously discussed.

5) *Stirring, slag removal, and aeration equipment:* All equipment used for stirring, slag removal, and aeration is coated with graphite and dried using a torch to eliminate moisture. This precaution is crucial because liquid aluminum is highly reactive to hydrogen gas.

6) *Mold paint:* For enhancing gloss and heat resistance, mold surfaces are painted with materials such as graphite powder, charcoal powder, or glass water. This coating aids in releasing the cast aluminum from the mold surface effectively.

7) *Pouring mold*: Two types of molds are prepared for research and comparison purposes: a large cast (~9kg) and a small cast (~2kg). The mold cavities are coated with graphite to easily remove solidified aluminum samples. Graphite's low

wettability with aluminum ensures the sample does not adhere to the mold walls after solidification. The design of metal molds for large and small batches is depicted in Fig. 1 [50].



Fig. 1 Metal molds are designed for large and small batches [50]

8) *Gas*: Industrial Argon (Ar) gas is used. Aeration with Ar gas breaks down dendritic structures and facilitates de-aeration. Combined with gentle stirring and oscillation of the liquid-slag interface, degassing helps achieve uniform composition throughout the batch.

9) *Pouring tube and pouring bowl*: During pouring, the method involves bottom-up pouring through a tube. This approach enhances productivity and improves the surface quality of ingots by allowing the steel water surface to rise steadily without splashing, which helps gases, impurities, and slag float to the top more effectively. It also facilitates the placement of an anti-reoxidation barrier.

10) *Slag filter*: A slag filter blocks light non-metallic impurities that float on the surface during pouring. This allows clean metal to flow through the gaps into the mold, ensuring high-quality castings.

### B. Melting and Denaturation Process

Here are the steps for arranging and drying ingredients in the process:

1) *Preparation of Utensils*: Ensure the furnace, pot, and other utensils are prepared and ready for use.

*Placing Aluminum Billet*: Place the chopped aluminum billet into the pot. Add the cryolite so that when the metal melts, a slag layer forms.

2) *Drying Intermediate Ingredients*: Place zinc, magnesium, intermediate alloys, and cryolite salt on the furnace lid for drying.

3) *Melting Aluminum Billet*: Once the aluminum billet has melted completely, gradually add the required pure metals by pressing them into the molten aluminum.

4) *Flow of Intermediate Metals*: Allow the intermediate metals and alloys to flow entirely into the melt.

5) *Aeration Process*: Initiate aeration with low flow (approximately 1 liter/min) for 2-3 minutes. Gentle stirring should be applied to avoid strong surface fluctuations and to ensure separation of liquid and slag phases, preventing outside gases from entering.

6) *Slag Removal*: Remove the slag from the surface after completing the aeration process.

7) *Raising Heat*: Increase the heat to reach the denaturation temperature, compensating for any heat loss during operation.

These steps ensure the proper preparation, melting, and treatment of ingredients to achieve consistent and high-quality results in the aluminum processing procedure [36], [50], [56].

8) *Pouring Liquid Metal*: Pour the metal at a temperature of 750°C quickly to minimize heat loss and ensure a stable flow of liquid metal.

9) *Solidification*: Allow the poured liquid metal to solidify within the mold.

10) *Mold Removal*: Remove the mold from the solidified metal after solidification.

11) *Sample Preparation*: Cut the solidified metal into small samples suitable for microscopic examination and durability testing.

12) *Sample Grouping*: Divide the samples into groups based on whether they are unmodified or modified, and further categorize them by whether they were cast in large or small molds. This process ensures the samples are prepared and categorized effectively for subsequent analysis and testing to evaluate their microscopic structure and durability characteristics.

### C. Heat Treatment Process

To achieve uniform incubation, follow these steps:

1) *Incubation Temperature*: Set the temperature to 480°C in the furnace.

2) *Heat Retention*: Maintain this temperature for 16 hours to ensure consistent incubation.

3) *Cooling Process*: After incubating, allow the sample to cool gradually in the same furnace. Ensure the sample temperature stabilizes with the ambient temperature before removing it from the furnace.

These steps ensure that the sample undergoes a controlled incubation process, followed by a gradual cooling phase, crucial for achieving uniform and reliable experimental conditions.

## III. RESULTS AND DISCUSSION

### A. Influence of Alloying Elements

Adding copper to an Al-Zn-Mg alloy can significantly enhance its strength. Here are the specifications with the alloy element ratios considered in the annealed state:

- Zinc (Zn): 4.0-10.0%
- Magnesium (Mg): Less than 6.5%
- Copper (Cu): Approximately 3.0%

In the annealed state, the alloy typically exhibits the following mechanical properties:

- Ultimate Tensile Strength (durability limit): 200-290 MPa
- Yield Strength (limit flow): 100-180 MPa
- Elongation: Greater than 10%

The addition of copper within these compositional ranges enhances the alloy's mechanical properties, particularly its strength and durability while maintaining good elongation characteristics suitable for various applications [57]–[59].

In heat-treatable Al-Zn-Mg-Cu alloys, the composition of zinc (Zn) and magnesium (Mg) plays a critical role in determining mechanical properties, especially in the heat treatment process involving quenching and aging [60]–[62]. Zn and Mg are highly soluble in aluminum at high temperatures and precipitate sharply during cooling, significantly strengthening the alloy when quenched and aged. Copper enhances the quenching effect but has minimal impact on aging performance [63]–[65]. The highest durability limit is typically achieved with around 2% copper, increasing relative elongation. For alloys containing 6-7% Zn and 2% Mg, increasing copper content to 3% further boosts durability and significantly enhances fatigue resistance. Higher levels (6-8%) increase durability but decrease alloy ductility and impact toughness. Zinc also reduces resistance to stress corrosion cracking more than magnesium. Content ranging from 1.5% to 3% varies based on desired mechanical properties. Higher magnesium levels above 2.5% notably reduce alloy ductility. Industry guidelines set upper limits for Zn and Mg to balance achieving the required strength against potential reductions in ductility, impact toughness, corrosion resistance, and fatigue resistance.

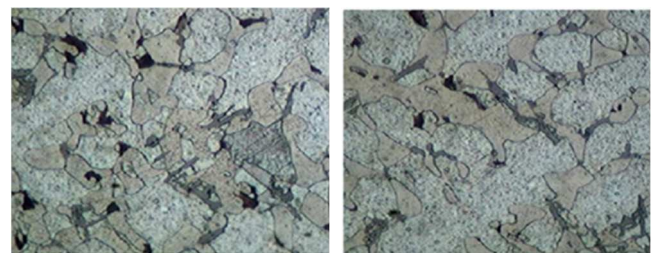
Understanding these relationships allows for optimizing Al-Zn-Mg-Cu alloy compositions to meet specific strength and performance requirements while managing potential trade-offs in other mechanical properties [57], [66]–[73]. The Al-Zn-Mg-Cu alloy is a high-strength aluminum alloy with versatile properties suitable for various industrial applications. Comprising zinc (Zn), magnesium (Mg), and copper (Cu), this alloy achieves remarkable strength. Its yield limit is only 20-30 MPa lower than its durability limit, surpassing common aluminum alloys like Duxra D16 in aging conditions by 40-50%. It exhibits superior durability limit and abrasion resistance compared to forged aluminum alloys such as AK6 and AK8. This makes it ideal for applications requiring high deformation capability while maintaining durability. Zn and Mg are key alloying elements with high solubility in aluminum. Their maximum solubility concentrations in aluminum are 82% for Zn and 17.4% for Mg, enabling effective strengthening through solid solution strengthening and precipitation hardening mechanisms. The alloy is suitable for deformation processing, surface heat treatment, and cutting machining, enhancing its versatility and applicability across various manufacturing processes. Overall, the Al-Zn-Mg-Cu alloy represents a robust choice for industries demanding high mechanical performance, durability, and processing flexibility in aluminum applications [74]–[80]. You seem to refer to the intermetallic

phases that form in Al-Zn-Mg-Cu alloys. These phases determine the alloy's properties and heat treatment stability. Here are some typical intermetallic phases found in these alloys. The  $\eta$  Phase ( $MgZn_2$ ) phase forms primarily with magnesium and zinc. It contributes to strengthening the alloy through precipitation hardening mechanisms. The T-phase ( $Al_2Mg_3Zn_3$ ) phase involves specific ratios of aluminum, magnesium, and zinc. It also enhances the alloy's mechanical properties, particularly in heat-treated conditions. The S Phase ( $Al_2CuMg$ ) is formed with aluminum, copper, and magnesium. This phase contributes to strengthening and stability during heat treatment. The  $\theta$  Phase ( $Al_2Cu$ ) phase involves aluminum and copper, providing additional strengthening through precipitation hardening. These intermetallic phases strengthen the alloy and contribute to its heat treatment stability by forming stable structures that resist changes at high temperatures. Their presence and distribution in the alloy matrix are crucial in achieving desired mechanical properties such as strength, toughness, and corrosion resistance in Al-Zn-Mg-Cu alloys.

TABLE II  
PHASES IN AL-ZN-MG AND AL-CU-MG ALLOYS [13], [14], [16], [23]

Phase	Al-Zn-Mg Alloy	Al-Cu-Mg Alloy
$\theta$		$Al_2Cu$
Z	$Mg_2Zn_{11}$	$Cu_6Mg_2Al_5$
S	-	$Al_2CuMg$
T ( $\tau$ )	$AlMgZn$ ( $Al_2Mg_3Zn_3$ ; $Al_6Mg_{11}Zn_{11}$ ; ( $Al, Zn$ ) $_{49}Mg_{32}$ )	$CuMg_4Al_6$
$\eta$ (M, $\sigma$ )	$MgZn_2$	$Al_6Cu_4Mg_2$

According to the research results of Isadare et al. [82], in Al-Zn-Mg-Cu alloys, the morphology of the  $MgZn_2$  ( $\eta$ ) phase can vary significantly depending on the cooling rate: Slow Cooling (a) and Fast Cooling (b). These differences in phase morphology between slow and fast cooling rates impact the mechanical properties and heat treatment response of the Al-Zn-Mg-Cu alloy. Microstructure of Al-Zn-Mg-Cu alloy is depicted in Fig. 2. At the same time, controlled cooling rates can be used to manipulate the distribution and size of these intermetallic phases, thereby optimizing the alloy's performance characteristics for specific applications.



a) Slow cooling b) Fast cooling

Fig. 2 Microstructure of Al-Zn-Mg-Cu alloy [82]

According to Fan et al. [73], various intermetallic phases can form during solidification in Al-Zn-Mg-Cu alloys and influence the alloy's properties. SEM image of Al-Zn-Mg-Cu alloy in the cast state is illustrated in Fig. 3. Here are some typical intermetallic phases:  $MgZn_2$  ( $\eta$ ) Phase;  $Al_2Mg_3Zn_3$  (T) Phase;  $AlCuMg$  (S) Phase;  $Al_2Cu$  ( $\theta$ ) Phase;  $Al_7Cu_2Fe$  and  $Al_{13}Fe_4$  Phases;  $Mg_2Si$  Phase. Research by Fan and others highlights the complex microstructure of Al-Zn-Mg-Cu

alloys, emphasizing the presence of these intermetallic phases and their distribution within the alloy matrix. Understanding their formation and morphology is essential for tailoring alloy

compositions and processing conditions to achieve desired mechanical and performance characteristics.

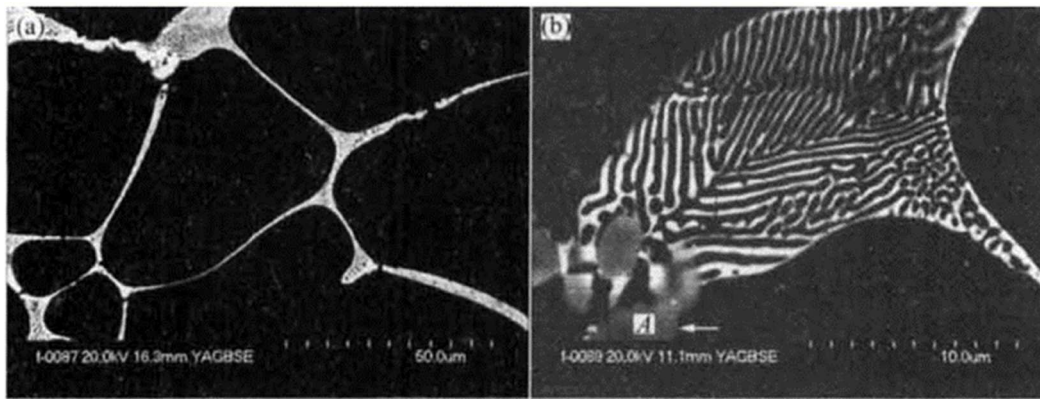


Fig. 3 SEM image of Al-Zn-Mg-Cu alloy in the cast state [73]

In Fig.4, the ratio of alloying elements, particularly the Mg/Zn ratio, significantly influences the formation of the  $MgZn_2$  phase, which acts as the primary chemical stabilizer in the Al-Zn-Mg-Cu aluminum alloy system [81]. Here are key points about the alloy's composition and properties. Zn and Mg are highly soluble in aluminum at high temperatures but precipitate sharply upon cooling, enhancing the alloy's strength significantly through quenching and aging processes. Alloys with Zn content ranging from 5.0% to 9.0% show optimal durability when quenched. Copper enhances the

quenching effect but has minimal impact on aging performance. Higher Zn content (6-8%) increases the durability limit of the alloy but reduces its ductility. Magnesium content typically ranges from 1.5% to 3%, depending on the desired mechanical properties. Above 2.5%, magnesium notably decreases the alloy's ductility. These insights underline the importance of precise control over alloy composition to tailor mechanical properties to specific application requirements in various industrial sectors.

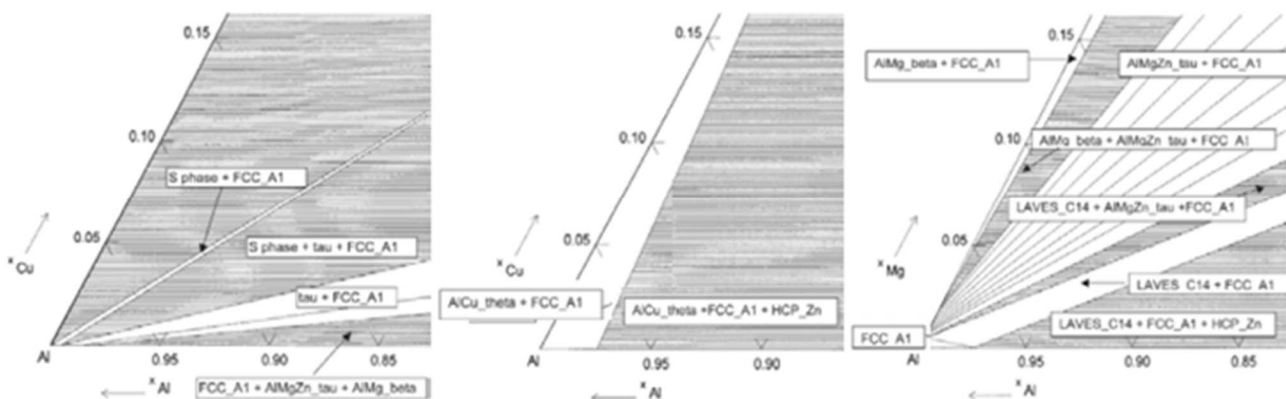


Fig. 4 Al-Cu-Mg alloy ternary phase diagram; Al-Cu-Zn and Al-Mg-Zn at 400°K [81]

In the Al-Zn-Mg-Cu alloy system, the addition of copper (Cu) significantly impacts the alloy's mechanical properties. Here are key points about the role of Cu and the resulting properties of the alloy. As Cu content increases in the Al-Zn-Mg-Cu system, some Zn in the T phase ( $Al_2Mg_3Zn_3$ ) is replaced by Cu. All three intermetallic phases (including the S phase  $Al_2CuMg$  and  $\theta$  phase  $Al_2Cu$  presented in Fig. 4) remain stable during aging. Adding Cu to the Al-Zn-Mg alloy increases the strength by approximately 20-50 MPa. With alloy compositions (Zn: 4.0-10.0%, Mg < 6.5%, Cu: 3.0%) in the annealed state, the durability limit ranges from 200-290 MPa, with a flow limit of 100-180 MPa and elongation more significant than 10%. The durability limit reaches its peak when the Cu content is about 2%, enhancing relative elongation. For alloys containing 6-7% Zn and 2% Mg,

increasing Cu content to 3% further boosts the durability limit and significantly improves the fatigue limit.

### B. Influence of other Alloying Elements

The Al-Zn-Mg-Cu system is often alloyed with additional elements such as Mn, Cr, Zr, and Ti. The elements Cr, Mn, and Zr accelerate the decomposition process of solid solutions, make particles more minor, and raise the recrystallization temperature. Therefore, adding Cr, Mn, and Zr stabilizes and causes a structural stabilizing effect shown in the Al-Zn-Mg-Cu-Sc-Zr alloy phase diagram (Fig. 5) [81]. In addition, transition metal elements improve granularity upon crystallization and enhance corrosion resistance under stress. When present in alloys, transition metals such as Cr, Mn, and Zr enormously change the organization in terms of phase distribution and the shape of grain boundaries. On the

one hand, transition metal elements promote the secretion of  $\eta$ , T, and S phases from the  $\alpha$  solid solution in a fine, dispersed state; on the other hand, they create a jagged and elongated shape on the boundary. the total boundary of the  $\alpha$  particle. With this characteristic organization, the intensity of corrosion cracking is reduced, and the rate of development of corrosion cracks along grain boundaries is also hindered, preventing corrosion cracking. Manganese increases the quenching effect to about 60 MPa and the aging effect to about 50 MPa. The maximum processing heat effect is nearly 100 MPa with 0.6% Mn. With 0.3% Cr, the alloy structure will not recrystallize, and fatigue strength will also increase significantly.

In the Al-Zn-Mg-Cu alloy system, additional alloying elements such as Mn, Cr, and Zr significantly enhance the alloy's properties. Here's how these elements affect the alloy. Manganese increases the quenching effect by about 60 MPa and the aging effect by about 50 MPa. The maximum processing heat effect is nearly 100 MPa with 0.6% Mn. With 0.3% Cr, the alloy structure resists recrystallization, significantly increasing fatigue strength. Along with Cr and Mn, Zr accelerates the decomposition process of solid solutions, making particles smaller and raising the recrystallization temperature. This has a stabilizing effect and enhances structural stability.

When adding Cr, Mn, and Zr, the alloy improves granularity upon crystallization and enhances stress corrosion resistance. Promote the secretion of  $\eta$  ( $MgZn_2$ ), T ( $Al_2Mg_3Zn_3$ ), and S ( $Al_2CuMg$ ) phases from the  $\alpha$  solid solution in a fine, dispersed state. In Fig.6, the microstructure of the alloy at annealing showed the S phase [81] Creating jagged and elongated grain boundary shapes reduces the intensity of corrosion cracking and hinders the development of corrosion cracks along grain boundaries. Including Mn, Cr,

and Zr in the Al-Zn-Mg-Cu alloy system demonstrates a strategic approach to optimizing the alloy's performance for demanding industrial applications, where enhanced strength, stability, and corrosion resistance are critical.

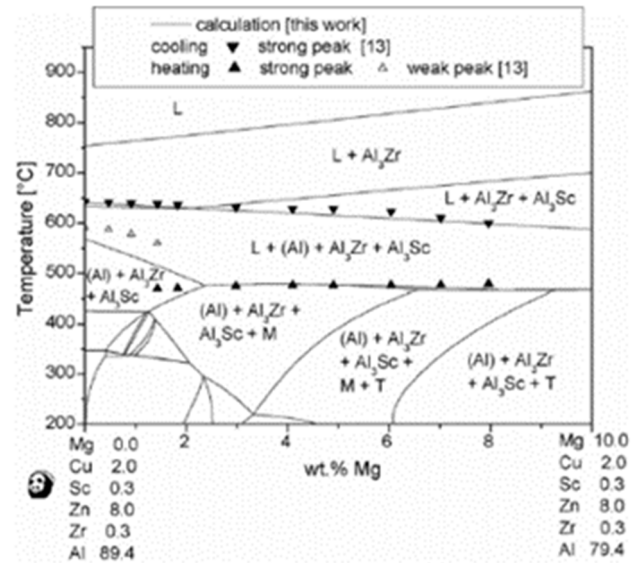


Fig. 5 Al-Zn-Mg-Cu-Sc-Zr alloy phase diagram [81]

Iron and silicon impurities in aluminum alloys lead to the formation of insoluble residual intermetallic compounds such as  $Al_6FeCuZn$ ,  $Al_7Cu_2FeZn$ ,  $Al_6MnFeCuCr$ , and  $Mg_2Si$ . These compounds precipitate from the liquid phase during crystallization, forming coarse particles. These particles act as stress concentrators, which can initiate microscopic cracks, reducing the alloy's ductility, impact toughness, and fatigue resistance. Hence, controlling impurities is crucial.

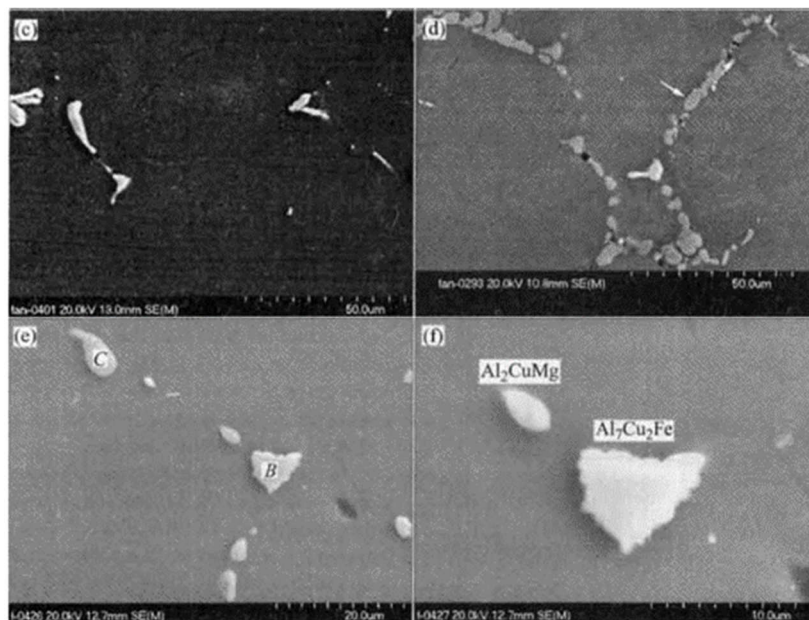


Fig. 6 Microstructure of alloy when annealed: alloy with Cu content < 2% (c; e) and with Cu content > 2% (d and f) [81]

### C. Research on Modification with Rare Earths

The research group of Nie et al. [32] studied the influence of the rare earth element erbium (Er) on some aluminum

alloys' microstructure and mechanical properties, including Al and Al-Mg alloys. In Fig. 7, increasing Er increases the hardness and strength due to forming the  $Al_3Er$  phase. As shown in Fig. 8, in Al – Cu alloy, the alloy's branch structure

is finely chopped when Er is added to the alloy. The recrystallization temperature increases, although the strength remains unchanged. In Fig.7 and Fig.8, the formation of the  $Al_8Cu_4Er$  phase has a low melting temperature, which reduces the formation of the  $CuAl_2$  phase - the main stable chemical element.

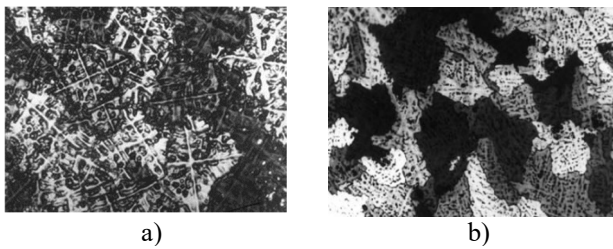


Fig. 7 Microstructure of Al-Mg - Er alloy after casting. Al - 5Mg (a), Al - 5Mg - 0.5Er (b) [32]

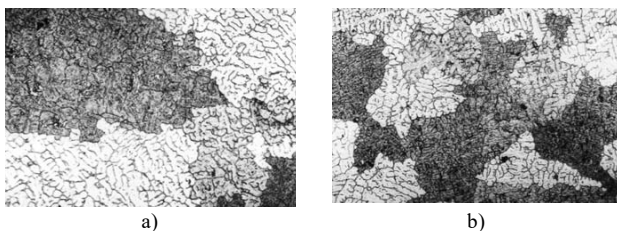


Fig. 8 Microstructure of Al - Cu alloy after casting. Al - 4Cu (a), Al - 4Cu - 0.2Er (b) [32]

Al - Zn - Mg and Al - Zn - Mg - Cu: The tensile strength  $\sigma_b$  and yield stress  $\sigma_{0.2}$  of the Al - Zn - Mg alloy increase rapidly when adding Er, while the elongation decreases slightly, the strength increases the most when adding 0.1% Er. Increasing the amount of Er will continue to increase strength, but the increase will decrease. The microstructure becomes much smoother, and the branch structure almost disappears. This can be explained by the formation of a small, fine  $Al_3Er$

phase, which plays a role as a crystallization nucleation zone. Similar results for Al - Zn - Mg - Cu alloy.

According to He et al. [83], the result presented the influence of Sc and Zr on Al-Zn-Mg-Cu alloy. By OM, which is shown in Fig. 9, the microstructure of this alloy is presented. The alloy is completely melted and then poured into a cold mold. After being thermally homogenized at 400°C for 5 hours, 450°C for 20 hours, and 470°C for 12 hours, the billets were quenched in water and kept at 420°C for 2 hours, then rolled into 4 mm thick sheets. The tensile test specimen was heat treated at 470°C for 2 hours, kept at 480°C for 1 hour, and finally quenched in water. The study results are summarized as follows: Adding 0.18% Zr to Al - Zn - Mg - Cu alloy castings will reduce grain fineness to a certain extent, with an average grain size of 80 - 130  $\mu m$ . The grain structure is a mixture of fibers and a small number of coaxial grains. Partial recrystallization occurs during hot rolling. Strength increased by 99 MPa, and elongation increased by 3.6%. Adding 0.18%Sc to Al - Zn - Mg - Cu composite castings reduces grain size. The microstructure consists of coaxial grains, and recrystallization occurs during hot rolling. Tensile strength increased by 166 MPa, and elongation increased by 9.2%. The main stabilization mechanism is the excreted  $Al_3Sc$  phase, dislocation blocking elements, and dislocation cutting of dispersed particles. Given both Sc and Zr, strong grain reduction and small equiaxed grains are obtained. The grain structure includes complete fiber organization; strength increases to 148.83 MPa and elongation up to 7.67%. Strength and elongation increase with the addition of Sc. The main stabilization mechanisms are particle smoothing, stabilization of the matrix structure, and shear deflection of dispersed particles. If both Zr and Sc are added simultaneously, the grain size will be finer many times due to the  $Al_3(Sc_xZr_{1-x})$  phase secretion mechanism on the Al-alpha base, shown in Fig. 10.

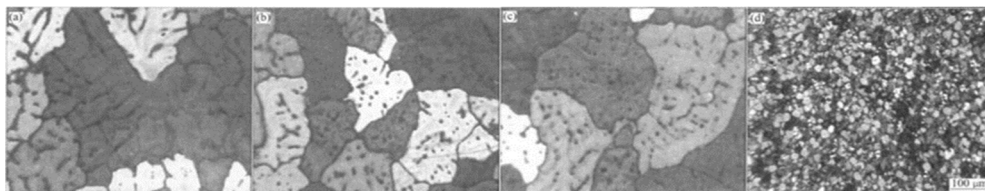


Fig. 9 Microscopic image (a) Al-Zn-Mg-Cu; (b) Al-Zn-Mg-Cu-0.18Zr; (c) Al-Zn-Mg-Cu-0.18Sc; (d) Al-Zn-Mg-Cu-0.30Sc-0.18Zr [83]

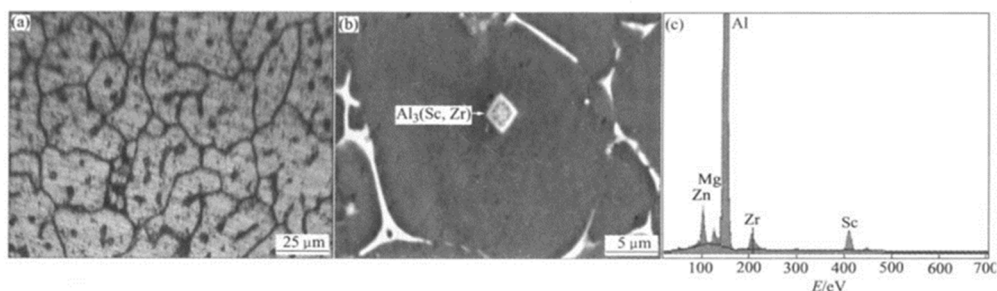


Fig. 10 SEM image and EDX analysis [83]

Zr occupies most of the center of the particles, while Sc surrounds the outside of the particles. The chemical formula of the known compound  $Al_3(Sc_xZr_{1-x})$ . The  $Al_3Zr$  phase is secreted first. Then, the  $Al_3Sc$  phase is secreted on the  $Al_3Zr$  surface; then the  $Al_3Zr$  phase is secreted again on the  $Al_3Sc$  substrate. Just like that, many layers will eventually overlap

with each other. The second phase is the seed center of  $\alpha$ -Al during solidification. When adding both Zr and Sc to the above alloy at the same time, smooth, round particles are formed, causing both the strength and elongation of the Al alloy to increase [84]-[87].

TEM analysis results show that Fig. 11a structure contains Zr. Many dispersed phases are clearly visible in both Fig. 11a and Fig. 11b. When adding Zr and Sc simultaneously, the secretion of the phase increases and reduces the size of the secreted phase. Fig. 11c showed coffee bean-like deformation in contrast to the phase and EDP secretion in Fig. 11d [83].

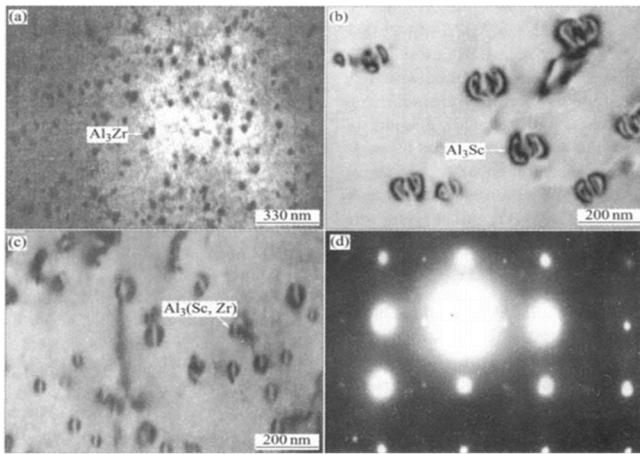


Fig. 11 TEM of  $Al_3Zr$ ,  $Al_3Sc$  v $\grave{a}$   $Al_3(Sc, Zr)$  in studying alloy: (a) Al-Zn-Mg-Cu-0.18%Zr; (b) Al-Zn-Mg-Cu-0.18%Sc; (c) Al-Zn-Mg-Cu-0.2%Sc-0.18%Zr; (d) EDP of (c) [83]

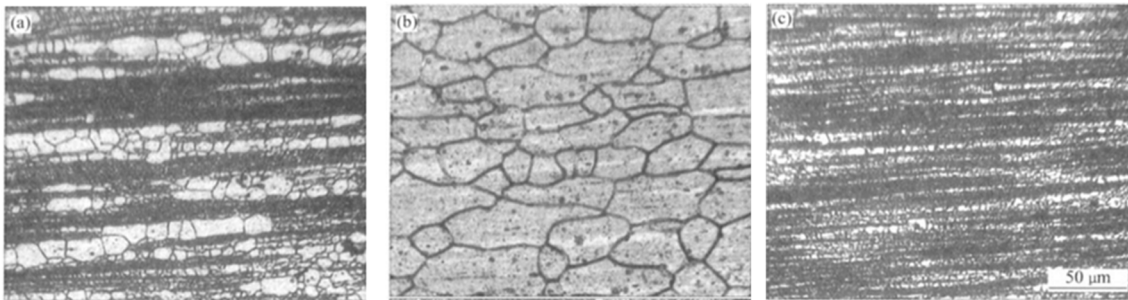


Fig. 12 Microstructure of alloy after hot rolling: (a) Al-Zn-Mg-Cu-0.18%Sc; (b) Al-Zn-Mg-Cu-0.18%Zr; (c) Al-Zn-Mg-Cu-0.1%Sc-0.18%Zr [83]

In addition, combination of the results from the bright region and dark central superlattice in the TEM images of sub-nano  $Al_3(Sc_{1-x}Zr_x)$  particles by high ductility reflection (110) (Fig. 13d and Fig. 13g), it is possible that the  $Al_3(Sc_{1-x}Zr_x)$  particles strongly hinder dislocation movement (indicated by yellow arrows) and grain/subgrain boundary displacement (indicated by white arrows). Furthermore, due to the strong influence of dislocations or grain boundaries in the deformation zone, the Ashby – Brown contrast of  $Al_3(Sc_{1-x}Zr_x)$  elements along with the precipitation process occurs and thus, the dislocation density decreases sharply (Fig. 13(e&f) and Fig. 13 (h&i)) [88]. It can be concluded that during deformation,  $Al_3(Sc_{1-x}Zr_x)$  grains play an important role in hindering dynamic recrystallization and grain enlargement [89].

During high ductility deformation, the grain size in the Al – Zn – Mg alloy increased rapidly to 15.4  $\mu m$ , and small subgrains were formed within the initial recrystallized grains. Compared with the fine grain surface in the Al – Zn – Mg alloy (Fig. 14(a&b)), grain boundary sliding can be observed in the Al – Zn – Mg – Sc – Zr alloy. At the peak stress stage of deformation, the deformed grains elongate with the rolled texture having recovered and partially recrystallized (Fig. 14(c&d)).

In Fig. 12, For Zr-containing alloys, recrystallization occurs where the density of the  $Al_3Zr$  dispersed phase is low during deformation and heat treatment [83]. This phenomenon is related to Zr in grains or grain boundaries; where Zr reduces the amount of solute available for phase secretion, the  $Al_3Zr$  dispersed phase will be depleted. Therefore, the weak recrystallization nucleation inhibits phase secretion during the hot rolling and aging process. Recrystallization occurs first in the  $Al_3Zr$ -poor region. The grain structure with the addition of 0.30% Sc and 0.18% Zr will form a complete fiber, and there will be no recrystallization during the hot rolling process [50], [83], [85], [86]. Studies on the effects of Sc and Zr to modify Al - Zn - Mg alloy, creating the  $Al_3(Sc_{1-x}Zr_x)$  phase on the Al( $\alpha$ ) base [35,43,45,46]. As observed in the bright area of the TEM image (Fig. 13(a-c)), in the early deformation stage ( $\epsilon = 0.69$  or 1.10), secondary circular  $Al_3(Sc_{1-x}Zr_x)$  nanoparticles are located at the boundary. The grain boundaries and the contrasting Ashby – Brown deformation zone (indicated by the blue arrow) show that these grains maintain a binding relationship with the Al( $\alpha$ ) matrix. Increasing the strain level to 2.4, the contrast of the irregular deformation region of  $Al_3(Sc_{1-x}Zr_x)$  nanograins in the highlight image suggests that as their size increases, the connectivity gradually decreases.

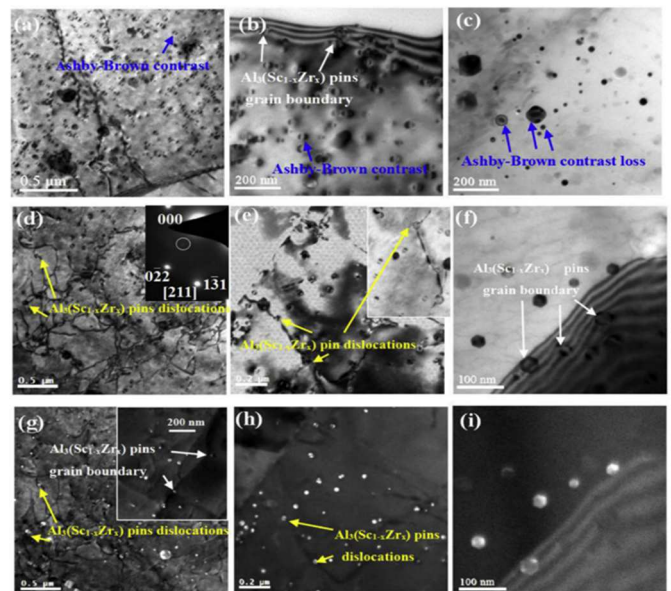


Fig. 13 TEM image of microstructure of  $Al_3(Sc_{1-x}Zr_x)$  nanoparticles during high plasticity deformation at 500oC and 0.01s-1,  $\epsilon=0.69$ ; (a) and (d) bright area image, (g) dark area image with superlattice in the center,  $\epsilon=1.10$ ; (b) and (e) bright area images, (h) (110) dark area images with super gill in the center;  $\epsilon=2.40$ : (c) and (f) bright area images, (i) (110) dark area images with superlattice in the center [88].

Furthermore, the fine particles with rolled texture accumulate a lot of energy, especially the S and Copper faces, which gradually escape and begin to form surrounding parent particles. Higher deformation storage. When straining to a true strain of 1.10, it is clear that large regions of recrystallized grains with S and Brass faces have formed and the grain size continues to increase (Fig. 14e). At the softening stage ( $\epsilon=2.40$ ), the normal organization consists of extremely fine and uniform micro-sized recrystallized particles (particle size  $<5\mu\text{m}$ ) with random arrangement (Fig. 14f&g). The fine grain size can be attributed to the Zener stopper from the secondary nano  $\text{Al}_3(\text{Sc}_{1-x}\text{Zr}_x)$  grains at the demigrain or grain boundaries, and the uniform grains from the generation of the selective limit of the nucleation center and growing by nano  $\text{Al}_3(\text{Sc}_{1-x}\text{Zr}_x)$  particles in high ductility deformation. Therefore, secondary nano  $\text{Al}_3(\text{Sc}_{1-x}\text{Zr}_x)$  particles are important in accelerating grain boundary deformation and achieving high ductility at high strain rates. The authors concluded that secondary  $\text{Al}_3(\text{Sc}_{1-x}\text{Zr}_x)$  nanoparticles only affect the dynamic softening deformation mechanism of the Al - Zn - Mg alloy. During the deformation hardening stage, the studied alloy is mainly controlled by the shear-driven dislocation creep mechanism. During the dynamic softening stage, the grain boundary sliding mechanism is dominant in the Al - Zn - Mg alloy with secondary  $\text{Al}_3(\text{Sc}_{1-x}\text{Zr}_x)$  nanoparticles [50], [88].

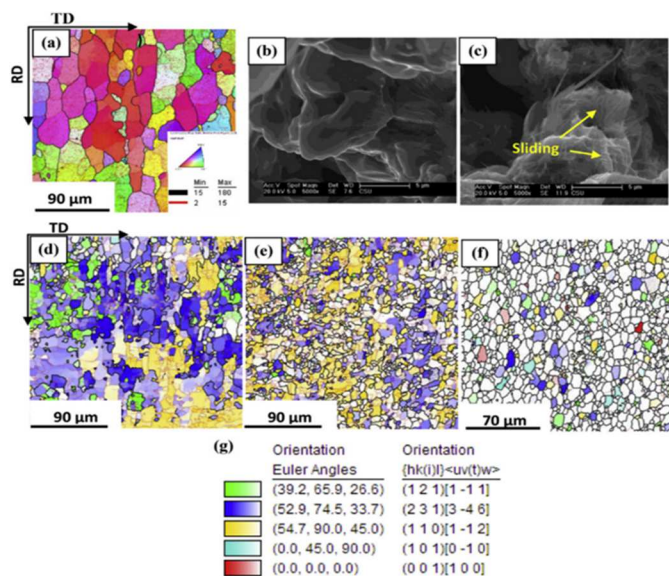


Fig. 14 EBSD, TEM, and SEM microstructure images of the two alloys under different real deformations at 500oC and 0.01s-1, the Al-Zn-Mg alloy deformed to destruction ( $\epsilon\sim 1.10$ ) : (a) EBSD mapping, (b) SEM fracture surface; Al-Zn-Mg-Sc-Zr alloy: (c) SEM fracture image, EBSD arrangement map (d)  $\epsilon = 0.69$ , (e)  $\epsilon = 2.40$ , (g) color equivalent to arrangement different in Figure 2.5 (d)-(f), the strength of the color reflects the deviation from the ideal arrangement [88]

According to Zhang et al. [88], Al-0.3Mg alloy was cast into 0.1 to 0.5 RE-modified specimens according to the conventional method. The study results are shown in Fig.15: The  $\alpha$ -Al phase is the dominant phase with a fractional peak in all the alloys studied. The  $\text{Al}_8\text{Mg}_5$  and  $\text{FeAl}_3$  phases are

found in Al-3.0%Mg alloys with 0 and 0.1% RE additions. The intensity of the  $\text{Al}_4\text{Ce}/\text{Al}_4\text{La}$  phases increased while the  $\text{Al}_8\text{Mg}_5$  and  $\text{FeAl}_3$  phases disappeared when the RE content increased to 0.2%. Thus, Al-Mg alloy can effectively remove Fe impurities and limit the formation of  $\text{Al}_8\text{Mg}_5$ . The addition of lanthanum and cerium can improve the solid solubility of magnesium into aluminum and reduce the formation of compounds  $\text{Al}_8\text{Mg}_5$ .

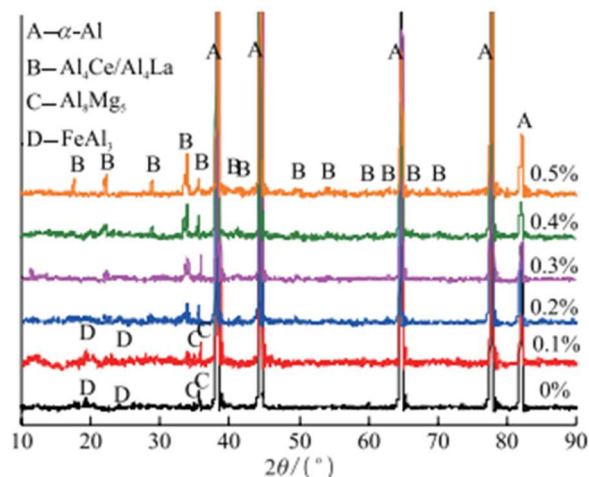


Fig. 15 Sample of XRD [88]

Through the EDS imaging results in Fig. 16, with the Al-0.3Mg alloy without RE added, the oxides make up the majority of the alloy weight, but when RE is added, the oxides are no longer found, proving that rare earth elements are capable of Deoxidation on molten aluminum base. The addition of rare earths refines the particle size. The second phases are concentrated at the grain boundaries and dispersed within the grains during solidification. La and Ce promote branch growth.  $\text{Al}_4\text{Ce}$  and  $\text{Al}_4\text{La}$  will form in molten aluminum and play a role in increasing the heterogeneous particles. In addition, increasing RE reduces porosity, possibly because La and Ce have reacted with hydrogen in molten aluminum to create stable  $\text{CeH}_2$  and  $\text{LaH}_2$  to eliminate air bubbles and porosity in the alloy. Adding Lanthanum and Cerium improves the tensile strength of Al-0.3Mg alloy. With the addition of rare earths, the tensile strength reaches its highest value at 0.3%RE. At that time, the tensile strength increased from 177MPa to 220MPa. However, the elongation is significantly reduced compared to 0.2%RE.

From the studies conducted, it has been observed that Al-Zn alloys are commonly modified with Zr or a combination of Zr and Sc. Chinese researchers have also explored using the rare earth element Er to modify Al-Zn alloys. Adding small amounts of rare earth or transition elements helps refine the alloy's grain structure. This is achieved through intermetallic phases that prevent the formation of detrimental phases such as  $\text{CuAl}_2$ . These intermetallic phases tend to concentrate at the center or surround the grains, inhibiting their growth. As a result, the alloy exhibits a finer grain structure, and the dendritic structure diminishes, leading to improved ductility and elongation.

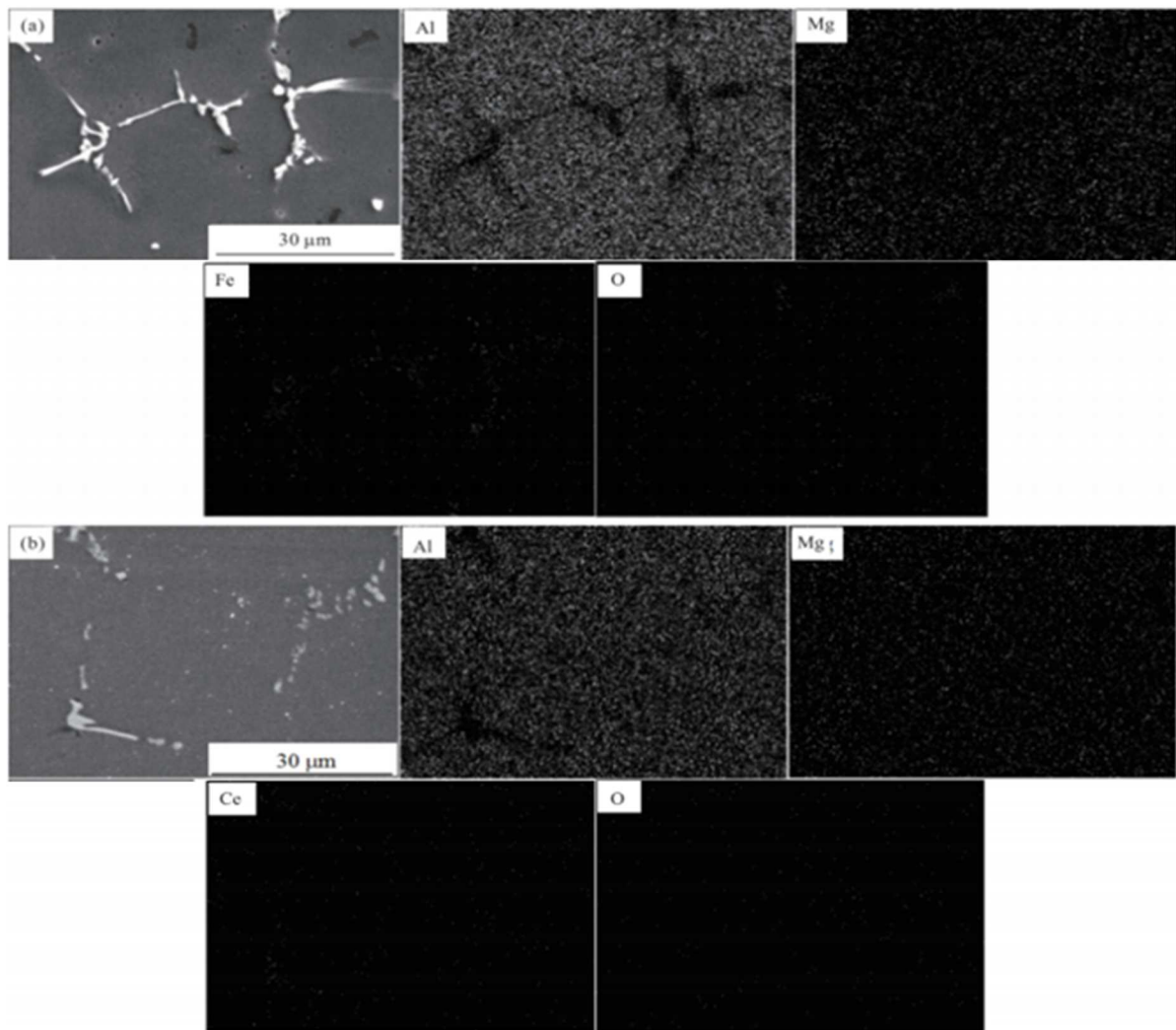


Fig. 16 EDS (a): 0%RE and (b) 0.2%RE [88]

#### D. Analysis of Structure Changes in Al-Zn-Mg-Cu Alloy after Casting

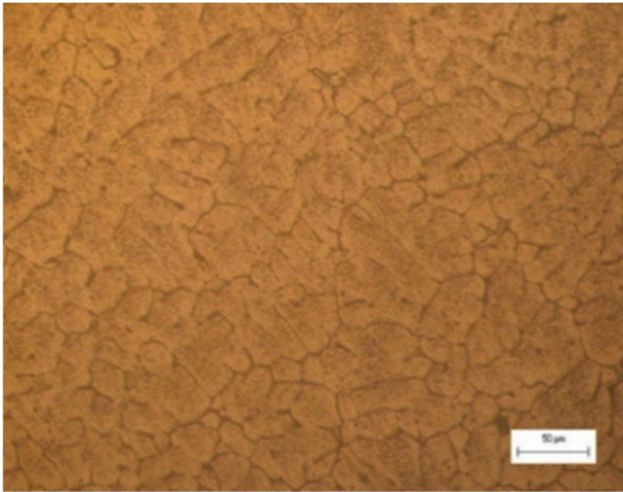
Upon examining Sample 1, it is evident that it does not exhibit the coarse grains typically associated with La or Ce, nor does it display large or uneven grains. The sample's microstructure, characteristic of the post-molding state, shows a tree-branch shape. However, after introducing La and Ce as grain-refining agents, the grain size significantly decreased compared to the unmodified sample. The grains became more uniform and finer, with sizes comparable to samples that do not contain La or Ce. Specifically, the average grain size was reduced by 88% compared to the sample without La and Ce, suggesting that these two elements significantly influence the casting process. This finding aligns with the theoretical framework proposed by author Zhang Xin [5].

In Fig. 17, the alloy's microstructure is depicted, where the brown background phases represent the aluminum matrix. The black phases observed at the grain boundaries are likely the intermetallic phases, which could be either  $MgZn_2$  or  $Mg_3Zn_3Al_2$ . These intermetallic phases play a crucial role in the mechanical properties and overall behavior of the alloy [3]. Additionally, there is a contribution from intermetallic phases formed between Al, La, and Ce. This contribution will be analyzed in the subsequent sections through the results of

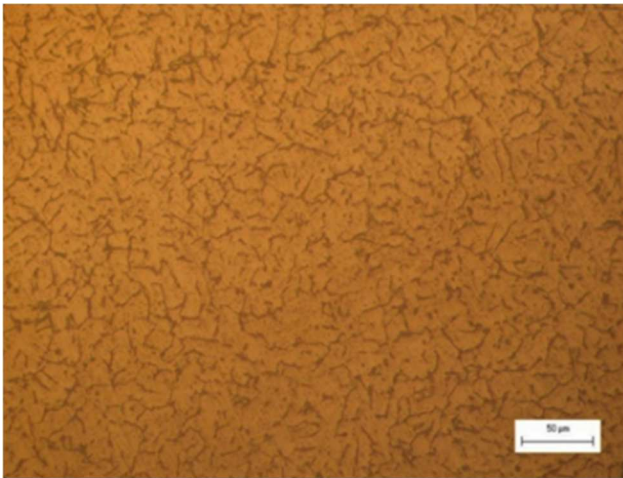
XRD diffraction analysis and SEM images of the sample. These analyses will provide detailed insights into the presence and distribution of these intermetallic phases and their impact on the alloy's microstructure and properties.

Without La and Ce: The distance between the branches of the alloy after casting without La and Ce is approximately 65  $\mu m$ . With La and Ce: This distance is reduced to 40-50  $\mu m$  for samples containing La and Ce. This reduction in branch size can be attributed to rare earth elements (RE)'s role in refining the alloy's microstructure. RE elements influence the grain structure, leading to finer branches. However, with the addition of RE elements in the studied alloy, intermetallic phases involving Al, and these elements may form. This hypothesis will be further validated through additional analyses such as XRD and SEM [50], SEM and EDS analyses of post-cast samples, as shown in Fig. 18 and Fig. 19, clearly evidence the formation of intermetallic phases between rare earth elements (RE) and aluminum.

The analysis of SEM and EDS, images at grain boundaries, confirms the presence of La and Ce within the composition at these boundaries. The role of these rare earth elements is significant, as they combine with other elements to form intermetallic phases that inhibit grain growth, thereby refining the alloy's microstructure.



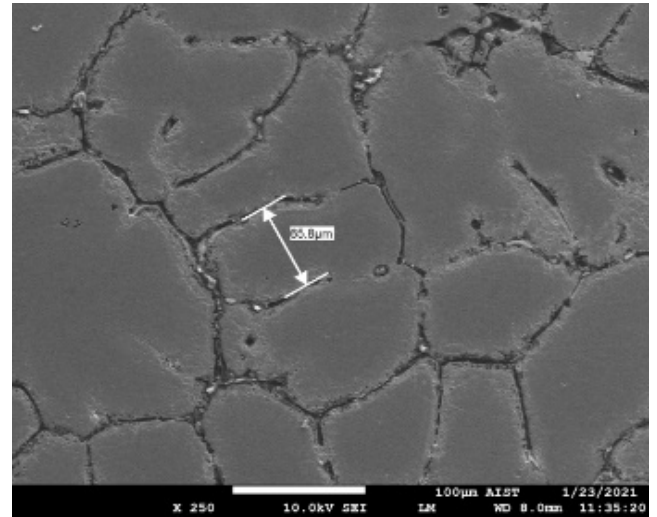
Sample 1



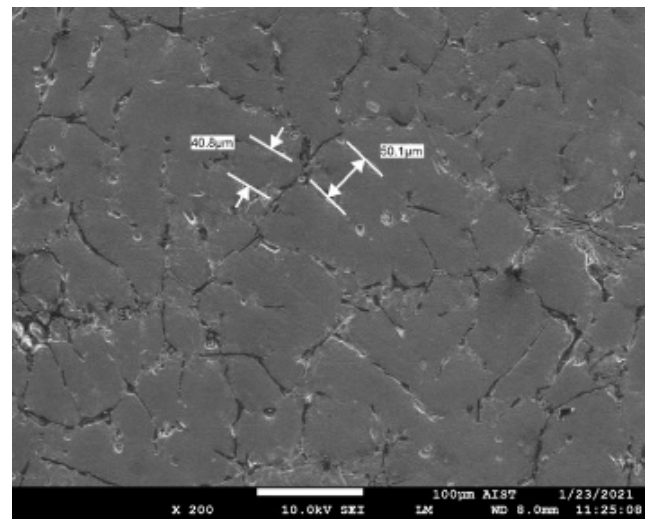
Sample 2

Fig. 17 Microscopic image results of the sample in the cast state, x200 [50]

In Fig. 18, it is crucial to conduct a more detailed SEM analysis to further understand the distribution of rare earth elements. This will determine whether the rare earth elements are primarily concentrated at the grain boundaries or if they are also present in the grain centers. Such detailed analysis will provide insights into the effectiveness of rare earth elements in modifying the alloy's microstructure and enhancing its properties [50]. According to [50], [90]–[92], the detailed SEM and EDS analyses reveal that rare earth elements are primarily concentrated at the grain boundaries. Consequently, intermetallic phases involving rare earth elements, specifically  $Al_x$  (La, Ce), are predominantly found at these grain boundaries. These intermetallic phases play a crucial role as blockers, effectively preventing the grain enlargement process and contributing to the refinement of the alloy's microstructure (Fig. 19). By concentrating on the grain boundaries, these  $Al_x$  (La, Ce) phases hinder the movement and growth of grains, thereby enhancing the mechanical properties of the alloy. This grain boundary pinning mechanism ensures that the grains remain fine and uniformly distributed, leading to improved ductility and strength [50].



Sample 1



Sample 2

Fig. 18 Analysis of the microstructure of the sample after casting (SEM image) [50]

Analyzing the sample results after adding denaturants, it is evident that rare earth elements are distributed across the entire surface of the phases, including both the background and the phase boundaries. The rare earth elements used as denaturants, such as La and Ce, do not dissolve in the liquid metal due to their higher melting temperatures than the denaturation temperature. Instead, they contribute to reducing energy required to form crystallization nucleation and crystals. Introducing rare earth elements into the Al-Zn-Cu-Mg alloy acts as foreign crystallization seed centers, resulting in a finer and smoother grain structure. The rare earth elements effectively inhibit the growth of primary crystals by providing numerous nucleation sites, leading to a more refined microstructure. This process enhances the mechanical properties of the alloy by creating a more uniform and fine-grained structure [50], [90], [93]–[96].

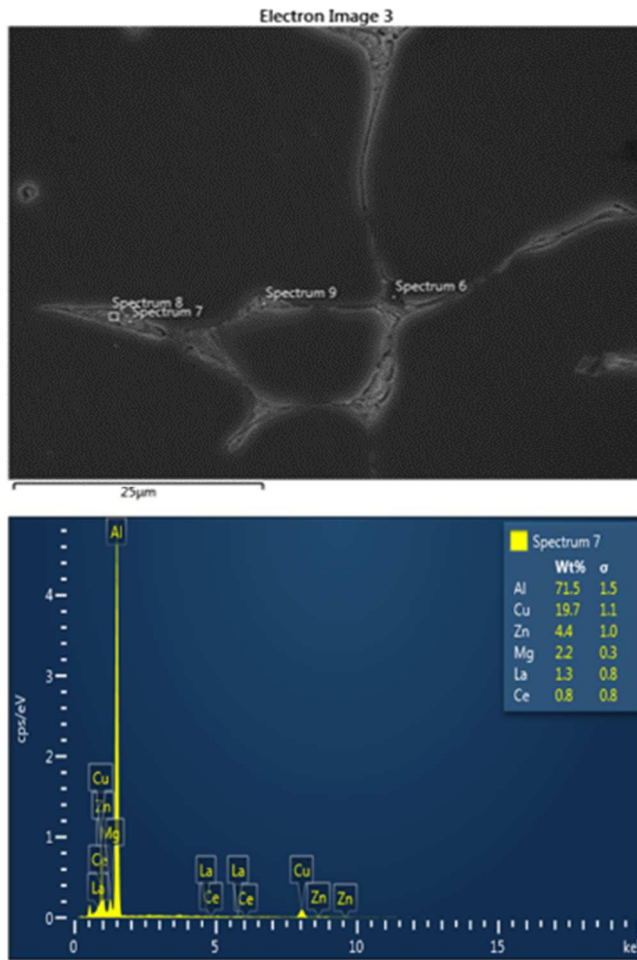
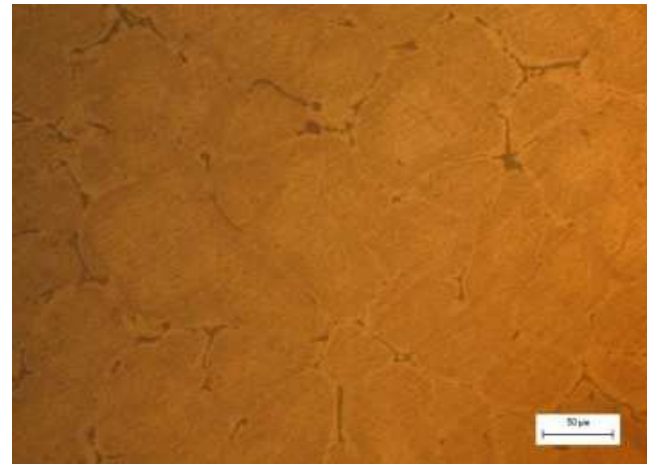


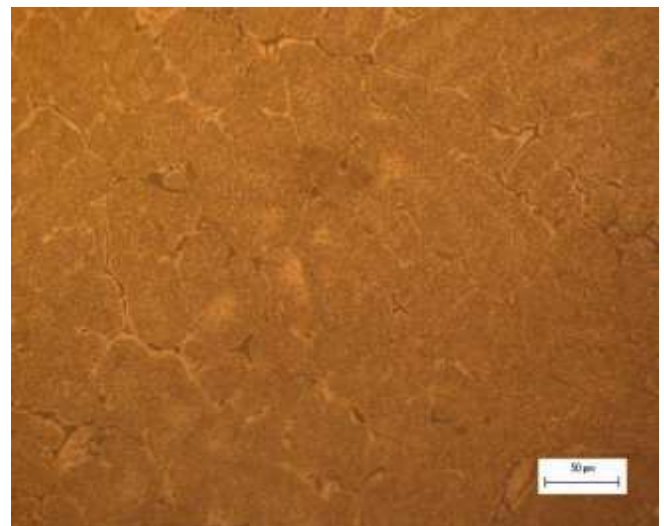
Fig. 19 SEM and EDS analysis of sample 2 [50]

Fig. 20 analyzes the sample's microstructure after uniform incubation at 480°C for 16 hours. It shows that the characteristic structure in the molded state (tree branch structure) of both sample 1 and sample 2 is no longer there. The black phases in the grain boundary region in the cast state of both samples have also gradually exuded into the aluminum matrix. This shows that this annealing regime is effective for 7475 alloys as demonstrated by the results of author Guillaume Fribourg [12]. In Fig. 20, the analysis of sample 1 without La and Ce reveals the following characteristics: These observations suggest that adding La and Ce is crucial in limiting grain growth during the heat treatment process. The formation of intermetallic phases involving rare earth elements effectively inhibits the growth of coarse grains, resulting in a finer and more uniform microstructure. This phenomenon is consistent with the documented findings by author Guillaume Fribourg, highlighting the effectiveness of rare earth elements in enhancing the microstructural stability and mechanical properties of the alloy after heat treatment [12]. According to [9], SEM results will provide a more detailed analysis due to their higher magnification capabilities than optical microscopes to clarify the presence of sub-particles in the boundary area with sizes ranging from 1-3 μm. These sub-particles are crucial for understanding the microstructural changes induced by rare earth elements (La, Ce). Regarding the black phases identified as MgZn<sub>2</sub> or Mg<sub>3</sub>Zn<sub>3</sub>Al<sub>2</sub>, which initially exist in the grain boundary region

of the sample in the cast state and have subsequently diffused into the aluminum matrix to form intermetallic phases with elements like Al, La, and Ce, this transformation will be thoroughly elucidated through XRD analysis results.



Sample 1



Sample 2

Fig. 20 Microstructure after annealing, x200 [50]

From the X-ray diffraction (XRD) pattern analysis in Fig. 21, it could be seen in Sample 1 (without La or Ce): In the post-cast state, no phases are observed that connect the elements Al, Zn, Mg, and Cu. The surface of the alloy primarily consists of aluminum. This indicates that without rare earth elements, the alloy does not form significant intermetallic phases involving these elements. In sample 2 (containing La and Ce), in the post-cast state, a small amount of AlCe phases is detected in sample 2 [50]. This suggests that adding an intermediate alloy between Al and rare earth elements (La, Ce) effectively modifies the Al-Zn alloy. The XRD results also show the presence of phases involving Mg-Al-Cu elements, such as Mg<sub>2</sub>Al<sub>3</sub> and S-(Al<sub>2</sub>CuMg), indicating that rare earths influence the phase formation of other elements in the Al-Zn alloy. After annealing, additional AlCe<sub>3</sub> phases appear in sample 2. This indicates that the annealing regime at 480°C for 16 hours effectively promotes the dispersion and interaction of rare earth elements with the aluminum substrate.

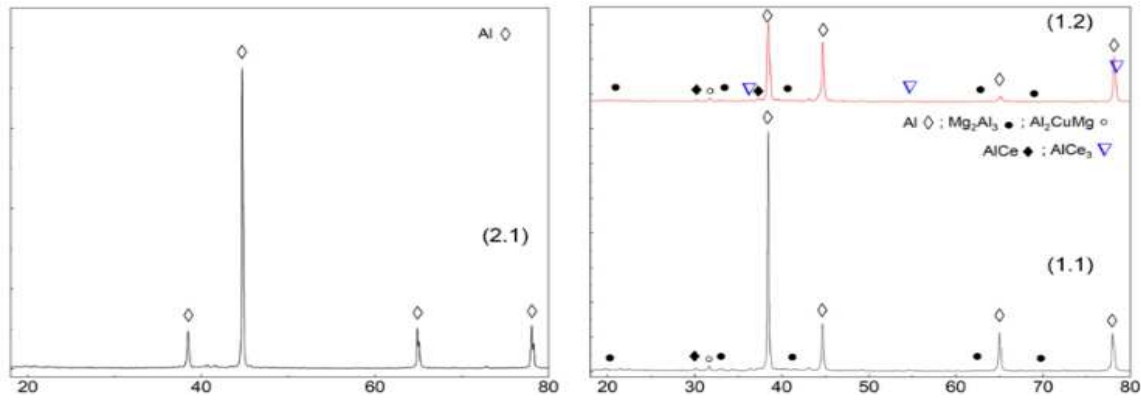


Fig. 21 XRD diffraction results, (2.1) Sample 1 in the post-cast state; (1.1) Sample 2 in the post-cast state; (1.2) Sample 2 is in the state after uniform annealing [50]

This aligns with findings from Guillaume Fribourg, suggesting that this annealing process optimally distributes rare earth elements on the aluminum surface. The XRD analysis confirms that incorporating rare earth elements (La, Ce) into the Al-Zn alloy leads to beneficial intermetallic phases, such as AlCe and AlCe<sub>3</sub>. These phases enhance the alloy's properties by influencing phase formation and distribution, particularly after annealing treatments. The results underscore the suitability of using intermediate alloys and specific annealing conditions to effectively modify and improve the microstructure and performance of Al-Zn alloys [40], [81], [97].

#### IV. CONCLUSION

The article compiles research demonstrating the significant role of alloying elements, particularly La and Ce, in shaping the microstructure of Al-Zn alloys. Intermetallic phases formed with La and Ce act as heterogeneous nucleation centers during crystallization or inhibit particle growth in the alloy. For instance, the Al<sub>11</sub>Ce<sub>3</sub> phase, present in intermediate alloys, resembles the  $\alpha$ -Al base phase and promotes the formation of fine grains. This results in a refined microstructure compared to alloys without La and Ce directly added. Al<sub>11</sub>Ce<sub>3</sub> phase acts as a seed center for crystallization, facilitating the formation of refined grains. While the Al<sub>3</sub>La phase prevents the development of  $\alpha$ -Al matrix phases, contributing to microstructural stability and refinement. The article highlights the effectiveness of uniform annealing processes for Al-Zn-Mg-Cu alloys containing La and Ce grain refiners. This annealing method eliminates the casting-induced microstructure, creating a more uniform organization. This uniformity is advantageous for subsequent deformation processes, enhancing the alloy's mechanical properties and structural integrity. Overall, the research underscores how the strategic addition of La and Ce, both directly and as intermediate alloys, influences the microstructural evolution of Al-Zn alloys. These elements play pivotal roles in grain refinement and phase control, ultimately improving the alloy's performance in industrial applications.

#### REFERENCES

- [1] X. D. Pham, A. T. Hoang, D. N. Nguyen, and V. V. Le, "Effect of factors on the hydrogen composition in the carburizing process," *Int. J. Appl. Eng. Res.*, vol. 12, no. 19, pp. 8238–8244, 2017.
- [2] D. N. Nguyen, A. T. Hoang, X. D. Pham, M. T. Sai, M. Q. Chau, and V. V. Pham, "Effect of Sn component on properties and microstructure CU-NI-SN alloys," *J. Teknol.*, vol. 80, no. 6, pp. 43–51, 2018, doi:10.11113/jt.v80.11867.
- [3] M. Abid, M. Kchaou, A. T. Hoang, and M. Haboussi, "Wear Mechanisms Analysis and Friction Behavior of Anodic Aluminum Oxide Film 5083 under Cyclic Loading," *J. Mater. Eng. Perform.*, vol. 33, no. 3, pp. 1527–1537, Aug. 2024, doi: 10.1007/s11665-023-08616-8.
- [4] X. . Pham, A. . Hoang, and D. . Nguyen, "A study on the effect of the change of tempering temperature on the microstructure transformation of Cu-Ni-Sn alloy," *Int. J. Mech. Mechatronics Eng.*, vol. 18, no. 4, pp. 27–34, 2018.
- [5] D.-T. Vo, D.-N. Nguyen, M.-T. Sai, Z. Said, X.-P. Nguyen, and D.-T. Nguyen, "A study of microstructure and properties of Cu-Ni-Sn alloy when deformation and aging," in *2022 Advances in Science and Engineering Technology International Conferences (ASET)*, 2022, pp. 1–6.
- [6] N. V. L. Le, D. N. Nguyen, A. T. Vu, D. T. Nguyen, and T. T. T. Tran, "Review on bainite phase transformation and mechanism in CMnSi steel," in *AIP Conference Proceedings*, 2023, vol. 2591, no. 1, p. 030082. doi: 10.1063/5.0119759.
- [7] H. Thi, N. Quyen, V. A. Tuan, T. P. Dong, V. V. Quyen, and N. D. Nam, "Effect of Rare Earth on M7C3 Eutectic Carbide in 13 % Chromium Alloy Cast Iron," *Int. J. Adv. Sci. Eng. Inf. Technol.*, vol. 9, no. 2, pp. 724–728, 2019.
- [8] D.-T. Vo, D.-N. Nguyen, T.-D. Nguyen, X.-P. Nguyen, Z. Said, and D.-T. Nguyen, "Influence of diffusion mode on microstructure and mechanical properties of carbonitriding layer," in *2022 Advances in Science and Engineering Technology International Conferences (ASET)*, 2022, pp. 1–7.
- [9] A. Tuan Hoang *et al.*, "Thermodynamic Simulation on the Change in Phase for Carburizing Process," *Comput. Mater. Contin.*, vol. 68, no. 1, pp. 1129–1145, 2021, doi: 10.32604/cmc.2021.015349.
- [10] T. Xuan Tran *et al.*, "Effect of Poly-Alkylene-Glycol Quenchant on the Distortion, Hardness, and Microstructure of 65Mn Steel," *Comput. Mater. Contin.*, vol. 67, no. 3, pp. 3249–3264, 2021, doi:10.32604/cmc.2021.015411.
- [11] P. K. Mallick, "Advanced materials for automotive applications: an overview," in *Advanced Materials in Automotive Engineering*, Elsevier, 2012, pp. 5–27. doi: 10.1533/9780857095466.5.
- [12] T. N. Le, M. K. Pham, A. T. Hoang, T. N. M. Bui, and D. N. Nguyen, "Microstructure change for multi-pass welding between Austenitic stainless steel and carbon steel," *J. Mech. Eng. Res. Dev.*, vol. 41, no. 2, pp. 97–102, Jan. 2018, doi: 10.26480/jmerd.02.2018.97.102.
- [13] T. N. Le, M. K. Pham, A. T. Hoang, and D. N. Nguyen, "Microstructures And Elements Distribution In The Transition Zone Of Carbon Steel And Stainless Steel Welds," *J. Mech. Eng. Res. Dev.*, vol. 41, no. 3, pp. 27–31, Sep. 2018, doi:10.26480/jmerd.03.2018.27.31.
- [14] A. . Hoang, V. . Le, A. . Nguyen, and D. . Nguyen, "A study on the changes in microstructure and mechanical properties of multi-pass welding between 316 stainless steel and low-carbon steel," *J. Adv. Manuf. Technol.*, vol. 12, no. 2, pp. 25–40, 2018.
- [15] M. K. Pham, D. N. Nguyen, and A. T. Hoang, "Influence of Vanadium Content on the Microstructure and Mechanical Properties of High-Manganese Steel," *Int. J. Mech. Mechatronics Eng.*, vol. 18, no. 2, pp. 141–147, 2018.

- [16] A. Hoang, D. N. Nguyen, and V. Pham, "Heat treatment furnace for improving the weld mechanical properties: Design and fabrication," *Int. J. Mech. Eng. Technol.*, vol. 9, no. 6, pp. 496–506, 2018.
- [17] A. T. Hoang, T. T. Van Tran, V. B. Nguyen, and D. N. Nguyen, "Effect of Heat Treatment Process on the Microstructure and Mechanical Properties of The Spray Coating Ni-Cr on CT38 Steel," *Int. J. Adv. Sci. Eng. Inf. Technol.*, vol. 9, no. 2, pp. 560–568, Mar. 2019, doi:10.18517/ijaseit.9.2.7891.
- [18] P. K. Krajewski, A. L. Greer, and W. K. Krajewski, "Main Directions of Recent Works on Al-Zn-Based Alloys for Foundry Engineering," *J. Mater. Eng. Perform.*, vol. 28, no. 7, pp. 3986–3993, Jul. 2019, doi:10.1007/s11665-019-04048-5.
- [19] Z. Song *et al.*, "Mechanism of room-temperature superplasticity in ultrafine-grained Al–Zn alloys," *Acta Mater.*, vol. 246, p. 118671, 2023.
- [20] Y. Reda, H. M. Yehia, and A. M. El-Shamy, "Microstructural and mechanical properties of Al-Zn alloy 7075 during RRA and triple aging," *Egypt. J. Pet.*, vol. 31, no. 1, pp. 9–13, 2022.
- [21] V. N. Chuvil'deev *et al.*, "Investigation of mechanical properties and corrosion resistance of fine-grained aluminum alloys Al-Zn with reduced zinc content," *J. Alloys Compd.*, vol. 891, p. 162110, Jan. 2022, doi: 10.1016/j.jallcom.2021.162110.
- [22] J. J. Xiao, C. Y. Liu, and K. Cao, "Effects of Cold Rolling on the Microstructure and Mechanical Properties of High-Zn-Content Al-Zn-Mg-Sc Alloys," *J. Mater. Eng. Perform.*, vol. 33, no. 3, pp. 1250–1261, 2024.
- [23] C. Xu, H. Teng, Y. Han, G. Jiang, H. Liu, and Y. Hu, "Experimental investigation and kinetic analysis of Al–Zn–Mg alloy coating," *Calphad*, vol. 84, p. 102655, 2024.
- [24] C. Chen *et al.*, "Phase transformation in Al/Zn multilayers during mechanical alloying," *Acta Metall. Sin. (English Lett.)*, vol. 36, no. 10, pp. 1709–1718, 2023.
- [25] E. AbdElRhiem, M. M. Mostafa, R. H. Nada, S. G. Mohamed, Y. F. Barakat, and S. M. Abdelaziz, "Effects of TiO<sub>2</sub>, CuO, and SiO<sub>2</sub> nanoparticles addition on the microstructure and mechanical properties of Al-10 wt% Zn alloy," *Phys. Scr.*, vol. 98, no. 6, p. 65018, 2023.
- [26] Q. Li, X. Ma, X. Zhang, J. Ma, X. Hu, and Y. Lan, "Microencapsulation of Al-Zn alloy as phase change materials for high-temperature thermal storage application," *Mater. Lett.*, vol. 308, p. 131208, 2022.
- [27] A. M. Abdel-Karim, A. M. El-Shamy, and Y. Reda, "Corrosion and stress corrosion resistance of Al Zn alloy 7075 by nano-polymeric coatings," *J. Bio-and Tribo-Corrosion*, vol. 8, no. 2, p. 57, 2022.
- [28] C. Chen and H. Zhang, "Characteristics of friction and wear of Al-Zn-Mg-Cu alloy after application of ultrasonic shot peening technology," *Surf. Coatings Technol.*, vol. 423, p. 127615, 2021.
- [29] N. Li, Z. Wei, W. Zhao, S. Yan, D. Liu, and Q. Jiao, "Improved ignition and combustion performance of Al-Zn-Mg ternary alloys by incorporating Mg into Al-Zn alloys," *Chem. Eng. J.*, p. 153237, 2024.
- [30] M. N. Borse, R. Bauri, and S. Shankar, "Study of microstructure evolution of friction stir welded novel (Al-Zn-Mg)-Fe (HE700) cast alloys for automotive applications," *Mater. Sci. Eng. A*, vol. 879, p. 145274, 2023.
- [31] R. G. Guan and D. Tie, "A review on grain refinement of aluminum alloys: Progresses, challenges and prospects," *Acta Metall. Sin. (English Lett.)*, vol. 30, no. 5, pp. 409–432, 2017, doi: 10.1007/s40195-017-0565-8.
- [32] Z. R. Nie *et al.*, "Advanced aluminum alloys containing rare-earth erbium," *Mater. Forum*, vol. 28, pp. 197–201, 2004.
- [33] N. LEY, "Superplasticity in structural materials," *Deform. Process. Struct. Mater.*, p. 284, 2005.
- [34] J. P. Abeyasinghe and E. G. Gillan, "Thermochemical reaction strategies for the rapid formation of inorganic solid-state materials," in *Dynamic Processes in Solids*, Elsevier, 2023, pp. 51–95.
- [35] F. Czerwinski, "Thermal stability of aluminum alloys," *Materials (Basel)*, vol. 13, no. 15, p. 3441, 2020.
- [36] N. H. Dung, *Modification of Aluminum alloy*, no. 04. Bach Khoa Publishing House, 2018.
- [37] N. H. Hài, *Rheocasting*. Bach Khoa Publishing House, 2017.
- [38] S. Kord, M. Alipour, M. H. Siadati, M. Kord, and P. G. Koppad, "Effects of extrusion and heat treatment conditions on microstructure and mechanical properties of an Al–Zn–Mg–Cu–Er alloy," in *Minerals, Metals and Materials Series*, 2018, vol. Part F4, pp. 1–26, doi: 10.1007/978-3-319-72284-9\_61.
- [39] H. Fang, H. Yang, J. Zhu, P. Xiao, Z. Chen, and T. Liu, "Effect of Minor Cr, Mn, Zr or Ti on Recrystallization, Secondary Phases and Fracture Behaviour of Al-Zn-Mg-Cu-Yb Alloys," *Xiyou Jinshu Cailiao Yu Gongcheng/Rare Met. Mater. Eng.*, vol. 49, no. 3, 2020.
- [40] G. R. Huang, Y. M. Sun, L. Zhang, and Y. L. Liu, "Effect of Trace Ce on Microstructure and Properties of Near-rapidly Solidified Al-Zn-Mg-Cu Alloys," *Cailiao Gongcheng/Journal Mater. Eng.*, vol. 46, no. 3, pp. 105–111, 2018, doi: 10.11868/j.issn.1001-4381.2016.000869.
- [41] S. K. Tian, J. Y. Li, J. L. Zhang, and D. Lü, "Effect of Sc on the microstructure and properties of 7056 aluminum alloy," *Gongcheng Kexue Xuebao/Chinese J. Eng.*, vol. 41, no. 10, 2019, doi:10.13374/j.issn2095-9389.2018.10.22.003.
- [42] P. S. Mohanty and J. E. Gruzleski, "Mechanism of grain refinement in aluminium," *Acta Metall. Mater.*, vol. 43, no. 5, pp. 2001–2012, 1995, doi: 10.1016/0956-7151(94)00405-7.
- [43] I. Z. Awan and A. Q. Khan, "Recovery, recrystallization, and grain-growth," *J. Chem. Soc. Pakistan*, vol. 41, no. 1, 2019, doi:10.52568/000707/jcsp/41.01.2019.
- [44] S. Li, Z. Huang, and S. Jin, "Superplastic behavioral characteristics of fine-grained 5A70 aluminum alloy," *Metals (Basel)*, vol. 9, no. 1, pp. 1–21, 2019, doi: 10.3390/met910062.
- [45] L. Bhatta, A. Pesin, A. P. Zhilyaev, P. Tandon, C. Kong, and H. Yu, "Recent development of superplasticity in aluminum alloys: A review," *Metals*, vol. 10, no. 1, pp. 1–26, 2020, doi:10.3390/met10010077.
- [46] O. A. Yakovtseva, A. V. Mikhaylovskaya, A. V. Pozdniakov, A. D. Kotov, and V. K. Portnoy, "Superplastic deformation behaviour of aluminium containing brasses," *Mater. Sci. Eng. A*, vol. 674, pp. 135–143, 2016, doi: 10.1016/j.msea.2016.07.053.
- [47] X. G. Wang, Q. S. Li, R. R. Wu, X. Y. Zhang, and L. Ma, "A Review on Superplastic Formation Behavior of Al Alloys," *Advances in Materials Science and Engineering*, vol. 2018, pp. 1–18, 2018, doi:10.1155/2018/7606140.
- [48] A. Mikhaylovskaya, O. Yakovtseva, M. Sitkina, and A. D. Kotov, "Grain-boundary and intragranular deformation in ultrafine-grained aluminum-based alloy at high strain rate," *Mater. Lett.*, vol. 276, pp. 128242 (1–5), 2020, doi: 10.1016/j.matlet.2020.128242.
- [49] O. D. Sherby and J. Wadsworth, "Superplasticity and superplastic forming processes," *Mater. Sci. Technol.*, vol. 1, no. 11, pp. 925–936, Nov. 1985, doi: 10.1179/mst.1985.1.11.925.
- [50] Bui Thi Ngoc Mai, "Influence of rare earth on high ductility of Al-Zn-Mg-Cu alloy," Hanoi University of Science and Technology, 2022.
- [51] George E. Dieter, *Mechanical metallurgy*. 1961.
- [52] Z. M. El-Baradie, "1998-Grain refining of Zn-22Al superplastic alloy.pdf," *Journal of Materials Processing Technology*, vol. 84, pp. 73–78, 1998.
- [53] M. F. Ibrahim, "Effects of Be, Sr, Fe and Mg Interactions on the Microstructure and Mechanical Properties of Aluminum Based Aeronautical Alloys," Université du Québec à Chicoutimi, 2015. [Online]. Available: <https://constellation.uqac.ca/id/eprint/3021/>
- [54] A. S. M. Handbook, *Alloy Phase Diagram*, vol. 3. 1992. doi:10.1007/BF02869318.
- [55] C. Tang, G. Zuo, Z. Li, X. Sun, and Q. Li, "An Overview on Alloying Research of Mg-Gd Alloys," *Cailiao Daobao/Materials Review*, vol. 32, no. 11, pp. 3760–3767, 2018, doi: 10.11896/j.issn.1005-023X.2018.21.012.
- [56] W. D. Callister, *Materials science and engineering: An introduction (2nd edition)*, vol. 12, no. 1. 1991. doi: 10.1016/0261-3069(91)90101-9.
- [57] K. Georgy, L. Neelakantan, K. C. H. Kumar, and M. Mukherjee, "Influence of Cu, Zn and Si alloying elements on Al alloy foams produced using Mg blowing agent," *J. Mater. Sci.*, vol. 56, no. 3, 2021, doi: 10.1007/s10853-020-05381-0.
- [58] M. Chemingui *et al.*, "Effect of heat treatment on microstructure, hardening and plasticity of a commercial Al–Zn–Mg–Cu alloy," *Int. J. Mater. Res.*, vol. 109, pp. 1113–1121, 2018.
- [59] J. Drápala, G. Kostíuková, and M. Losertová, "Contribution to the aluminum-tin-zinc ternary system," *IOP Conf. Ser. Mater. Sci. Eng.*, vol. 266, no. 1, pp. 0–16, 2017, doi: 10.1088/1757-899X/266/1/012002.
- [60] Q. Zhou, X. Xu, S. Yin, and T. Han, "A novel strategy to enhance the mechanical properties and corrosion resistance of ultra-high strength Al-Zn-Mg-Cu alloy: Pre-recovery Multi-Stage Solution Treatment (P-MST)," *Mater. Sci. Eng. A*, vol. 912, p. 146964, 2024.
- [61] J. Chu, T. Lin, G. Wang, H. Fang, and D. Wang, "Effect of Heat Treatment on Microstructure and Properties of Al-7.0 Zn-1.5 Cu-1.5 Mg-0.1 Zr-0.1 Ce Alloy," *Metallogr. Microstruct. Anal.*, vol. 9, pp. 312–322, 2020.
- [62] A. Beigi Kheradmand, S. Mirdamadi, Z. Lalegani, and B. Hamawandi, "Effect of thermomechanical treatment of Al-Zn-Mg-Cu with minor amount of Sc and Zr on the mechanical properties," *Materials (Basel)*,

- vol. 15, no. 2, p. 589, 2022.
- [63] Y. Dai, L. Yan, and J. Hao, "Review on micro-alloying and preparation method of 7xxx series aluminum alloys: progresses and prospects," *Materials (Basel)*, vol. 15, no. 3, p. 1216, 2022.
- [64] A. B. Kheradmand, M. Tayebi, M. M. Akbari, and A. Abbasian, "Effect of quench-controlled precipitation hardening on microstructure and mechanical properties of Al-Zn-Mg-Cu-Zr alloys contain of Sc micro-alloying," *J. Alloys Compd.*, vol. 902, p. 163748, 2022.
- [65] F. Jiang, J. Huang, Y. Jiang, and C. Xu, "Effects of quenching rate and over-aging on microstructures, mechanical properties and corrosion resistance of an Al-Zn-Mg (7046A) alloy," *J. Alloys Compd.*, vol. 854, p. 157272, 2021.
- [66] P. A. Rometsch, Y. Zhang, and S. Knight, "Heat treatment of 7xxx series aluminium alloys - Some recent developments," *Transactions of Nonferrous Metals Society of China (English Edition)*, vol. 24, no. 7. Nonferrous Metals Society of China, pp. 2003–2017, 2014. doi:10.1016/S1003-6326(14)63306-9.
- [67] V. V. Bryukhovetsky, D. E. Myla, V. P. Poyda, and A. V. Poyda, "Effect of Homogenization on the Superplasticity and Microsuperplasticity of the Al-Zn-Mg-Cu Aluminum Alloy," *J. Nano-Electron. Phys.*, vol. 12, no. 6, pp. 06025-1-06025-8, 2020, doi:10.21272/jnep.12(6).06025.
- [68] M. T. Pérez-Prado, M. C. Cristina, O. A. Ruano, and G. González-Doncel, "Grain boundary sliding and crystallographic slip during superplasticity of Al-5%Ca-5%Zn as studied by texture analysis," *Materials Science and Engineering A*, vol. 244, no. 2, pp. 216–223, 1998. doi: 10.1016/S0921-5093(97)00567-4.
- [69] H. Zhao *et al.*, "Segregation assisted grain boundary precipitation in a model Al-Zn-Mg-Cu alloy," *Acta Mater.*, vol. 156, pp. 318–329, 2018, doi: 10.1016/j.actamat.2018.07.003.
- [70] F. Carreño and O. A. Ruano, "Superplasticity of aerospace 7075 (Al-Zn-Mg-Cu) aluminium alloy obtained by severe plastic deformation," *Defect Diffus. Forum*, vol. 385 DDF, pp. 39–44, 2018, doi:10.4028/www.scientific.net/DDF.385.39.
- [71] X. Z. Li, V. Hansen, J. Gjénnnes, and L. R. Wallenberg, "HREM study and structure modeling of the Z' phase, the hardening precipitates in commercial Al-Zn-Mg alloys," *Acta mater*, vol. 47, no. 9, pp. 2651–2659, 1999.
- [72] R. xian YANG, Z. yi LIU, P. you YING, J. lin LI, L. hua LIN, and S. min ZENG, "Multistage-aging process effect on formation of GP zones and mechanical properties in Al-Zn-Mg-Cu alloy," *Trans. Nonferrous Met. Soc. China (English Ed.)*, vol. 26, no. 5, pp. 1183–1190, 2016, doi: 10.1016/S1003-6326(16)64221-8.
- [73] X. FAN, D. JIANG, Q. MENG, B. ZHANG, and T. WANG, "Evolution of eutectic structures in Al-Zn-Mg-Cu alloys during heat treatment," *Trans. Nonferrous Met. Soc. China*, vol. 16, no. 3, pp. 577–581, Jun. 2006, doi: 10.1016/S1003-6326(06)60101-5.
- [74] G. Sha and A. Cerezo, "Early-stage precipitation in Al-Zn-Mg-Cu alloy (7050)," *Acta Mater.*, vol. 52, no. 15, pp. 4503–4516, Sep. 2004, doi: 10.1016/j.actamat.2004.06.025.
- [75] L. Berg *et al.*, "GP-zones in Al-Zn-Mg alloys and their role in artificial aging," *Acta Mater.*, vol. 49, no. 17, pp. 3443–3451, Oct. 2001, doi: 10.1016/S1359-6454(01)00251-8.
- [76] A. A. Alekseev, I. N. Fridlyander, and L. B. Ber, "Mechanisms of phase transformations under ageing in the alloys of Al-Zn-Mg-(Cu) system," in *Materials Science Forum*, 2002, vol. 396–402, no. 2, pp. 821–826. doi: 10.4028/www.scientific.net/msf.396-402.821.
- [77] J. X. Zang, K. Zhang, and S. L. Dai, "Precipitation behavior and properties of a new high strength Al-Zn-Mg-Cu alloy," *Trans. Nonferrous Met. Soc. China (English Ed.)*, vol. 22, no. 11, pp. 2638–2644, Nov. 2012, doi: 10.1016/S1003-6326(11)61511-2.
- [78] L. L. Rokhlin, T. V. Dobatkina, N. R. Bochvar, and E. V. Lysova, "Investigation of phase equilibria in alloys of the Al-Zn-Mg-Cu-Zr-Sc system," in *Journal of Alloys and Compounds*, Mar. 2004, vol. 367, no. 1–2, pp. 10–16. doi: 10.1016/j.jallcom.2003.08.003.
- [79] T. Marlaud, A. Deschamps, F. Bley, W. Lefebvre, and B. Baroux, "Influence of alloy composition and heat treatment on precipitate composition in Al-Zn-Mg-Cu alloys," *Acta Mater.*, vol. 58, no. 1, pp. 248–260, Jan. 2010, doi: 10.1016/j.actamat.2009.09.003.
- [80] M. Chemingui *et al.*, "Effect of heat treatment on microstructure, hardening and plasticity of a commercial Al-Zn-Mg-Cu alloy," *Int. J. Mater. Res.*, vol. 109, no. 12, pp. 1113–1121, Dec. 2018, doi:10.3139/146.111709.
- [81] G. Fribourg, "Precipitation and plasticity couplings in a 7xxx aluminium alloy: application to thermomechanical treatments for distortion correction of aerospace component," Institut National Polytechnique de Grenoble, 2010.
- [82] A. M. O. A. A. R. O. K. M. R. A. L. A. K. . Isadare D.A, "Effect of As-Cast Cooling on the Microstructure and Mechanical Properties of Age-Hardened 7000 Series Aluminium Alloy," *Int. J. Mater. Eng.*, vol. 2015, no. 1, pp. 5–9, 2015, doi: 10.5923/j.ijme.20150501.02.
- [83] Y. D. He, X. M. Zhang, and J. H. You, "Effect of minor Sc and Zr on microstructure and mechanical properties of Al-Zn-Mg-Cu alloy," *Trans. Nonferrous Met. Soc. China (English Ed.)*, vol. 16, no. 5, pp. 1228–1235, 2006, doi: 10.1016/S1003-6326(06)60406-8.
- [84] T. G. L. Megumi Kawasaki, "Developing superplasticity and a deformation mechanism map for the Zn-Al eutectoid alloy processed by high-pressure torsion," *Mater. Sci. Eng. A*, vol. 528, pp. 6140–6145, 2011.
- [85] V. Kodetová *et al.*, "Phase transformations in commercial cold-rolled Al-Zn-Mg-Cu alloys with Sc and Zr addition," *J. Therm. Anal. Calorim.*, vol. 145, pp. 2991–3002, 2020, doi: 10.1007/s10973-020-09862-x.
- [86] A. Kishchik, A. Mikhaylovskaya, A. Kotov, and V. Portnoy, "Effect of homogenization treatment on superplastic properties of aluminum based alloy with minor Zr and Sc additions," *Defect Diffus. Forum*, vol. 385 DDF, pp. 84–90, 2018, doi:10.4028/www.scientific.net/DDF.385.84.
- [87] J. Liu *et al.*, "Effect of minor Sc and Zr on recrystallization behavior and mechanical properties of novel Al-Zn-Mg-Cu alloys," *J. Alloys Compd.*, vol. 657, pp. 717–725, 2016, doi:10.1016/j.jallcom.2015.10.122.
- [88] X. Zhang, Z. Wang, Z. Zhou, and J. Xu, "Influence of rare earth (Ce and La) addition on the performance of Al-3.0 wt%Mg alloy," *J. Wuhan Univ. Technol. Mater. Sci. Ed.*, vol. 32, no. 3, pp. 611–618, 2017, doi: 10.1007/s11595-017-1642-6.
- [89] R. Ohte, K. Yoshioka, T. Uesugi, Y. Takigawa, and K. Higashi, "Effects of Zr-addition on intergranular fracture of Al-Cu-Mg and Al-Zn-Mg-Cu alloys," *Keikinzoku/Journal Japan Inst. Light Met.*, vol. 69, no. 4, pp. 235–241, 2019, doi: 10.2464/jilm.69.235.
- [90] B. T. N. Mai, "Influence of Recrystallization Annealing on the Microstructure and Ductility of Al-Zn-Mg-Cu Alloy Added La, Ce," *Lect. Notes Mech. Eng.*, pp. 333–339, 2023, doi: 10.1007/978-3-031-31824-5\_40.
- [91] R. K. Mahidhara and A. K. Mukherjee, "Mechanisms of cavity growth in a fine-grained 7475 Al superplastic alloy," *Materials and Design*, vol. 16, no. 6, pp. 343–348, 1995. doi: 10.1016/0261-3069(96)00012-X.
- [92] H. Iwasaki, M. Mabuchi, and K. Higashi, "Plastic cavity growth during superplastic flow in AA 7475 Al alloy containing a small amount of liquid," *Acta Materialia*, vol. 49, no. 12, pp. 2269–2275, 2001. doi:10.1016/S1359-6454(01)00124-0.
- [93] D. A. Porter and K. E. Easterling, *Phase transformations in metals and alloys*. Chapman & Hall, 1992.
- [94] D. H. Shin, K. T. Park, and E. J. Lavernia, "High-temperature deformation in a superplastic 7475 Al alloy with a relatively large grain size," *Materials Science and Engineering A*, vol. 201, no. 1–2, pp. 118–126, 1995. doi: 10.1016/0921-5093(95)09761-9.
- [95] A. L. Vasiliev *et al.*, "Microstructural Peculiarities of Al-Rich Al-La-Ni-Fe Alloys," *Metall. Mater. Trans. A Phys. Metall. Mater. Sci.*, vol. 50, no. 4, pp. 1995–2013, 2019, doi: 10.1007/s11661-019-05127-x.
- [96] L. Li, T. T. Zhou, H. X. Li, C. Q. Chen, B. Q. Xiong, and L. K. Shi, "Effect of additional elements on aging behavior of Al-Zn-Mg-Cu alloys by spray forming," *Trans. Nonferrous Met. Soc. China (English Ed.)*, vol. 16, no. 3, pp. 532–538, 2006, doi: 10.1016/S1003-6326(06)60093-9.
- [97] Z. Geng, D. Xiao, and L. Chen, "Microstructure, mechanical properties, and corrosion behavior of degradable Mg-Al-Cu-Zn-Gd alloys," *J. Alloys Compd.*, vol. 686, no. C, pp. 145–152, 2016, doi:10.1016/j.jallcom.2016.05.288.